International Journal of Multiphase Flow 157 (2022) 104232

Contents lists available at ScienceDirect

International Journal of Multiphase Flow

journal homepage: www.elsevier.com/locate/ijmulflow

Settling of heavy cylindrical particles in granular beds

J.J. Derksen *

School of Engineering, University of Aberdeen, Aberdeen, United Kingdom

ARTICLE INFO

Keywords:
Particle-resolved simulation
Lattice-Boltzmann method
Granular bed
Sedimentation
Solid-liquid flow

ABSTRACT

The way a rigid cylindrical particle falls through a viscous Newtonian liquid into a loosely packed granular bed of smaller and lighter particles has been studied numerically. This solid-liquid flow system has been solved with the lattice-Boltzmann method combined with an immersed boundary method for explicitly imposing no-slip at the particle surfaces. We study the effect of the orientation of the cylinder (vertical and horizontal), its settling speed (the Reynolds numbers at impact is of the order of 100), and its density (relative to liquid and bed density) on the depth of penetration into the granular bed. The simulation results are particularly sensitive to the friction between particles as parameterized through friction coefficients (varied in the range 0.15 – 0.50). The results have practical relevance for particles getting immobilized – or even buried – in granular beds. More importantly, the simulation cases have been designed such as to allow for straightforward experimentation the results of which would be valuable for further numerical model development.

1. Introduction

Flow over granular beds – as in coastal regions and rivers but also in pipelines and agitated slurry reactors and crystallization reactors – is a topic of great practical relevance. As a result, there is a large body of literature on closely associated phenomena such as granular bed morphology and consistency, erosion, sediment transport, (re)suspension of solids, and particle-fluid interaction. This paper attempts to make a modest contribution to the general topic of granular bed dynamics by considering the fate of an intruding (or "alien") particle falling on a granular bed.

The overall aim of our research is to assess under what circumstances an alien particle is likely to get immobilized by – or even buried in – a granular bed. This has, for instance, relevance if the alien particle is a contamination (e.g. is a plastic waste particle) that we want to locate in an ecosystem. In this paper we develop a computational approach to investigate this research question. We appreciate that for gaining confidence in the computational approach it needs validation through experimentation. Therefore in this particular paper we study relatively simple situations that can be replicated fairly easily in a physical experiment. Experimental data then will be greatly beneficial for further model development and subsequently allow for simulating (combined with further experimentation) more complex cases.

The computational approach pursued here falls in the category of particle-resolved simulation. In particle-resolved simulation, the spatial resolution of the flow solution is finer than the size of the particles and therefore allows for explicitly applying the no-slip condition at solid particle surfaces. The forces and torques on the individual particles are part of the flow solution. This enables evolving the linear and angular dynamics of the particles which feeds back to the fluid flow as updated boundary conditions. Particle-resolved simulations are expensive on a per-particle basis. With spatial resolution requirements such that the spacing of the computational grid on which the fluid flow is solved is at least one order of magnitude smaller than the size of a suspended particle, one needs – in three dimensions – of the order of 10^3 to 10^4 grid points per particle so that only small-scale systems can be simulated. Particle-resolved simulations that contain up to order 10^6 particles have been reported (Kidanemariam and Uhlmann, 2017). Since the natural and engineered systems alluded to above contain many orders of magnitude more particles, particle-resolved simulations deal with sub-systems and are conducted primarily to reveal fluid-solid interactions at the micro scale. Over the past few decades, particle-resolved simulations involving spheres have provided valuable insights in fluid-solid drag forces (Hill et al., 2001; Rubinstein et al., 2016; Van der Hoef et al., 2005) as well as other momentum transfer mechanisms (Wylie et al., 2003), in fluidization and sedimentation (Derksen and Sundaresan, 2007) as well as in sediment transport (Kidanemariam and Uhlmann, 2014; Vowinckel et al., 2007). Given that particle-resolved simulations explicitly account for no-slip at the surface of a particle, they directly are able to account for the shape of a particle.

* Corresponding author.
E-mail address: jderksen@abdn.ac.uk.

https://doi.org/10.1016/j.ijmultiphaseflow.2022.104232
Received 20 April 2022; Received in revised form 8 July 2022; Accepted 21 August 2022
Available online 24 August 2022

Simulations involving non-spherical particles have – among more – been reported by Wachs (2009).

For reasons of computational efficiency, particle-resolved simulations are mostly carried out on a fixed grid on which the fluid flow is solved and an immersed boundary method to account for the presence of the particles (Uhlmann, 2005). Specifically for dense suspensions, a fixed-grid approach has important implications. In dense suspensions, particles are in close proximity and regularly (and inevitably) the spacing between two particle surfaces falls below the (fixed) grid spacing so that their hydrodynamic interaction is not well resolved. This lack of resolution is usually mitigated by including lubrication force models (Nguyen and Ladd, 2002), that are well established for spherical particles but less so for non-spherical particles (Wachs, 2019). Also "dry" (or direct) contact between particles requires a modeling approach to account for restitution and friction (Yamamoto et al., 2001). The modeling of close-range interactions between particles is an important and often times a somewhat speculative element of particle-resolved simulations for which support from experimental data is highly beneficial. For the systems considered in this paper, a realistic representation of dry friction between particles appears to be crucial.

This paper has been organized as follows. In the next section we define the flow systems that have been simulated. Then the simulations methodology is explained with an emphasis on the implementation of dry friction between particles. A base-case is defined in physical and numerical terms in the subsequent section where we also discuss the variations from the base-case that we have considered. We then present results of the simulations and – in the final section – draw conclusions.

2. Flow system

Impressions of the flow systems are given in Fig. 1. These are rectangular, three-dimensional domains of size $nx{\cdot}ny{\cdot}nz$ with a Cartesian coordinate system as defined in the figure. Gravity points in the negative z-direction: $\mathbf{g} = -g\mathbf{e}_z$. We have periodic boundary conditions in x and y direction. The lower and upper boundaries (at $z = 0$ and $z = nz$ respectively) are no-penetration, free-slip walls.

In the domain we place a loosely packed bed (solids volume fraction $\phi \approx 0.6$) of uniformly sized particles having density ρ_b. The particles are free to move and rotate except for a layer of particles closely above the $z = 0$ boundary that are held fixed. In most cases the bed consists of spheres all having the same diameter d_b (see the left panel of Fig. 1). The bed then comes up to a height of approximately $16d_b$. We also will be showing results for beds of cylindrical particles having a length over diameter ratio equal to 1 and a volume-equivalent diameter equal to d_b (see the right panel of Fig. 1).

In addition to the bed, the domain contains Newtonian liquid with density ρ and kinematic viscosity ν, and one alien particle. The latter is a solid rigid cylinder with density ρ_a, diameter d_a and length ℓ_a. It is released with zero velocity above the bed and is either oriented horizontally or vertically. The vertical distance from the lowest point of the alien particle to the upper surface of the bed we call h (as indicated in Fig. 1). The upper surface of the bed, at $z = z_{bs}$, is defined as the average of the z-coordinates of the centers of the 10 upper most bed particles.

The settling of the alien particle towards the granular bed we characterize by the Archimedes number, defined as $\mathrm{Ar} = (\gamma - 1)gd_a^3/\nu^2$ (with $\gamma = \rho_a/\rho$), and the Reynolds number of the cylinder at the moment of its first contact with the bed $\mathrm{Re}_i = |u_{zi}|d_a/\nu$ (with $|u_{zi}|$ the impact speed). Note that Re_i is not an input parameter. It can, however, be controlled through h. In this study, h is small enough for the cylinder not to change its orientation between release and impact with the bed.

The physical situation we have in mind is a bed of $d_b \approx 1$ mm particles in a watery liquid ($\nu \approx 10^{-6}$ m^2/s, $\rho \approx 10^3$ kg/m^3) with a density ratio $\rho_b/\rho \approx 1.1$ and an alien particle a cylinder with $d_a/d_b \approx 2$, $\ell_a/d_a \approx 4$, and ρ_a/ρ in the range 2 – 6. These physical parameters – along with $g = 9.8$ m/s^2 – guide the choices we made in the simulations for the Archimedes number, aspect ratios, and density ratios.

The parameters that govern close-range interaction between particles, including "dry" collision parameters, are difficult to accurately gauge experimentally. At the same time, we expect them to have an impact on the way the alien particle interacts with the bed; specifically when it comes to friction coefficients of which there are two (μ_{bb} between bed particles and μ_{ab} between alien particle and bed particles).

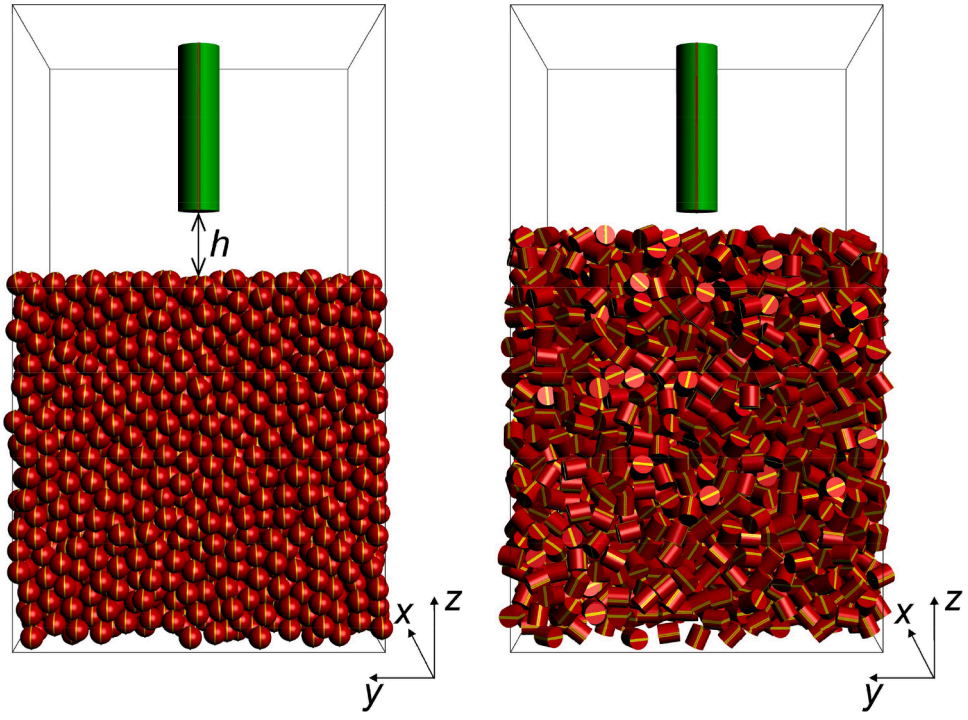

Fig. 1. Flow geometry and coordinate system. Left: Geometry with bed of spherical particles and alien cylinder at its initial position; right: bed of short cylindrical particles and alien cylinder at its initial position.

Furthermore there are restitution coefficients (e_{bb} and e_{ab}) and parameters governing close range lubrication forces. To limit the dimensionality of our parameter space we have set $e_{bb} = e_{ab} = 1$ justified by the fact that we have a solid-liquid system; the energy dissipated between two particles approaching through liquid dominates over the energy dissipated in the actual (dry) contact (Derksen and Sundaresan, 2007). Lubrication interactions and dry friction, and the way they have been implemented in the simulations, are discussed in the numerical methods part of the paper.

3. Numerical procedures

The simulations resolve the fluid flow down to a length scale finer by one order of magnitude than the size of the particles that constitute the bed and – in doing so – explicitly determine hydrodynamic forces and torques acting on the particles. The fluid flow is solved on a fixed uniform cubic grid with spacing Δ. Therefore, if surfaces of two particles are closer than Δ (which in the granular bed is the rule rather than the exception) the liquid flow as a result of relative particle motion is not fully resolved. As discussed above, to compensate for this lack of resolution we invoke lubrication force modelling (Nguyen and Ladd, 2002). This results in additional hydrodynamic forces (and potentially torques) acting on the particles. Hydrodynamic forces along with collisional forces and their resulting torques as well as net gravity drive the translational and rotational dynamics of the particles. We numerically solve Newton's (translation) and Euler's (rotation) equations of motion for each individual particle, i.e. we update their velocities, locations and orientations through time stepping. The so updated particle configuration then provides new boundary conditions for the fluid flow. Below we summarize the numerical approaches to perform the tasks as just described. Most of the approaches have been introduced in our previous papers (Derksen, 2019, 2022) with the exception of dry friction. For that reason, and because of its perceived effect on the settling processes, friction has been given a more detailed treatment in the current paper.

As the flow solver the lattice-Boltzmann method (Kruger et al., 2017; Succi, 2001) has been used, more specifically the scheme introduced by Somers (Somers, 1993). It operates on a uniform cubic lattice (spacing Δ) and evolves through time stepping with step size Δt. It has been coupled with an immersed boundary method (IBM) for imposing no-slip at the solid surfaces of the particles (Ten Cate et al., 2002). In the simulations, the surfaces are represented by closely spaced (nearest neighbor spacing $\sim 0.6\Delta$) off-grid marker points. At these points forces on the liquid are applied such that the liquid velocity (interpolated from the lattice) approaches the velocity of the solid surface thereby achieving no-slip (Ten Cate et al., 2002). The so determined force distribution over each particle surface is integrated to calculate the (resolved parts of) the hydrodynamic force and torque on the particle.

In addition to the resolved hydrodynamic forces (and resulting torques), three types of forces on the particles that are associated to close-range particle-particle interactions have been included in the simulations: (1) radial lubrication forces; (2) radial collision forces; (3) tangential collisions forces, i.e. friction. The detection of closeness and contact between two particle surfaces also makes use of marker points. When the distance between two marker points on two different particles falls below a threshold, first a lubrication force is activated. Upon closer approach also contact forces kick in. In this paper tangential lubrication forces are not considered.

The expressions as to how the radial lubrication and radial collision force depend on the relative location of the two marker points and – for lubrication – their relative velocity have been introduced previously, including parameter settings (Derksen, 2019). The inclusion of dry friction is new to our simulation procedure. The approach to friction is based on (Yan et al., 2015). First we briefly summarize radial lubrication and collision with reference to Fig. 2 that shows two marker points (1 and 2) on the surface of two different particles (A and B). When the distance δ as defined in Fig. 2 falls below the preset value δ_d and at the same time $\delta_\lambda < \lambda$ (δ_λ defined in Fig. 2, λ a preset distance) the radial lubrication force becomes active according to (Derksen, 2019)

$$\mathbf{F}_{12}^{n,lub} = k^n \left(\frac{1}{\delta} - \frac{1}{\delta_d}\right) \frac{|\delta_\lambda - \lambda|}{\lambda} \Delta\mathbf{u}^n \text{if} \delta < \delta_d \text{and} |\delta_\lambda| < \lambda; \quad \mathbf{F}_{12}^{n,lub} = \mathbf{0} \text{otherwise} \tag{1}$$

with $\Delta\mathbf{u}^n$ the relative velocity of marker points 1 and 2 along the average normal $\mathbf{n} = \frac{\mathbf{n_2}-\mathbf{n_1}}{|\mathbf{n_2}-\mathbf{n_1}|}$. Since this force is to account for hydrodynamic interactions unresolved by the lattice, the distances δ_d and λ have been set to values of the same order as the lattice spacing: $\delta_d = \lambda = \Delta$. For the interaction between two spheres with diameter d the expression for the coefficient k^n reads $k^n = \frac{3}{8}\pi\rho\nu d^2$ (Nguyen and Ladd, 2002). For interactions involving cylinders we use – for lack of a better model – the cylinder diameter in the latter expression.

When $\delta < \delta_0$ with $\delta_0 = 0.1\Delta$ (and if still $\delta_\lambda < \lambda$) we assume that a dry contact is taking place that we represent by a radial repulsive linear spring force

$$\mathbf{F}_{12}^{n,c} = k(\delta_0 - \delta) \frac{|\delta_\lambda - \lambda|}{\lambda} \mathbf{n} \text{if} \delta < \delta_0 \text{and} |\delta_\lambda| < \lambda; \quad \mathbf{F}_{12}^{n,c} = \mathbf{0} \text{otherwise} \tag{2}$$

with k the spring constant. It has been set such that the spring would be

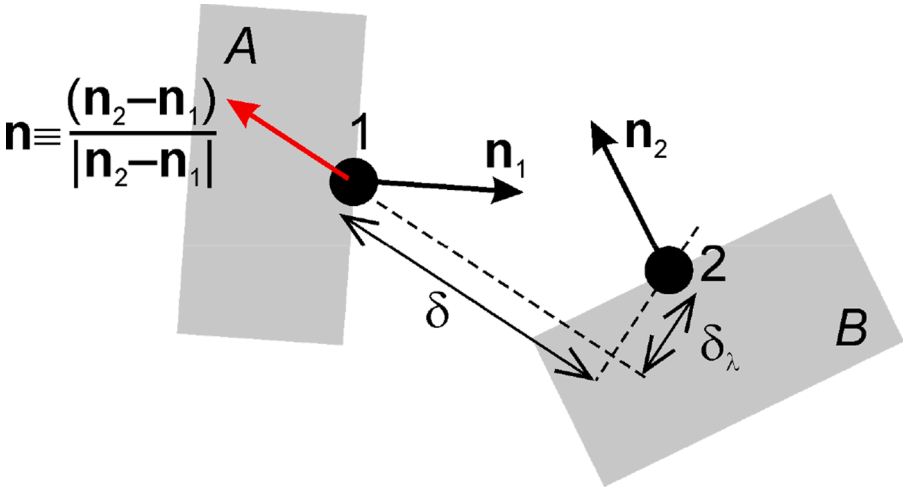

Fig. 2. Two marker points 1 and 2 on two different particles (A and B respectively) in close proximity. Definition of normal vectors and radial distance δ and lateral distance δ_λ.

compressed over a distance $0.6\delta_0$ if the spring would carry the net weight of a bed particle: $k = \frac{\pi}{6} d_b^3 (\rho_b - \rho) g / (0.6\delta_0)$.

The onset of the radial contact force also triggers the dry friction force by activating a spring in tangential direction. Each time step after its activation, until the contact gets deactivated, the tangential spring is stretched according to $\mathbf{s} = \int (\mathbf{u}_2 - \mathbf{u}_1 - \Delta\mathbf{u}^n)\, dt$ (Yan et al., 2015) with, in the simulations, the integral being a sum over the finite size time steps Δt. The associated friction force is

$$\mathbf{F}_{12}^{t,c} = k\mathbf{s} \quad \text{if } k|\mathbf{s}| \le \mu_{AB}|\mathbf{F}_{12}^{n,c}|; \quad \mathbf{F}_{12}^{t,c} = \mu_{AB}|\mathbf{F}_{12}^{n,c}| \frac{\mathbf{s}}{|\mathbf{s}|} \quad \text{if } k|\mathbf{s}| > \mu_{AB}|\mathbf{F}_{12}^{n,c}| \tag{3}$$

where we use the same spring constant k as for the radial contact force and introduce a friction coefficient μ_{AB} between particle A and B. In most cases we will only consider one overall friction coefficient μ. As mentioned above, in a few cases we have a friction coefficient among bed particles that is different from the one between a bed particle and the alien particle. The contact and lubrication forces are summed up per particle to get the total force and torque due to close-range interaction acting on each particle.

The equation of linear motion (Newton's 2nd law) contains the resolved hydrodynamic force, the close-range interaction forces and net gravity. The equation of angular motion (Euler equation) contains the resolved hydrodynamic torque and close-range interaction torques. We evolve these equations in time with an explicit split-derivative method (Shardt and Derksen, 2012) that uses the same time step Δt as the (lattice-Boltzmann) flow updates. The updates of particle orientation make use of quaternions (Kuipers, 1999).

4. Set-up of simulations

The random bed of spherical particles is created by randomly placing spheres in a non-overlapping manner in a domain with in x and y direction the same dimensions as the simulation domain (nx and ny respectively). These spheres are initially smaller than the spheres we are aiming for since purely random non-overlapping placement can only go up to a solids volume fraction of ~0.3 (Torquato et al., 2000). The spheres are then given random velocity to move as a hard-sphere granular gas (i.e. there is no interstitial liquid yet) with restitution coefficient one and friction coefficient zero. Each time step we grow all spheres by an amount equal to 50% of the smallest distance between two sphere surfaces in the entire domain at that moment. This we keep doing until we reach the target sphere diameter d_b and have reached a solids volume fraction of ~0.6. This assembly of spheres we place in the lower part of the $nx{\cdot}ny{\cdot}nz$ simulation domain. Liquid is added, gravity is activated and a two-phase simulation is started where the bottom layer of spheres (with thickness $1.5d_b$) is held fixed. This creates a rough, random bottom surface on which the rest of the spheres – that are free to move – settle. If we would let the spheres settle on a smooth, horizontal surface it would create some level of order in the arrangement of spheres which is not representative for a deep granular bed. Once this bed is settled, i.e. when fluid and particle velocities have become negligibly small, we are ready to add the alien cylindrical particle. A settled bed of spheres and the alien particles at its initial position are shown in Fig. 1, left panel.

It is somewhat more cumbersome to create a random, dense bed of cylinders. These cylinders have a length ℓ_c equal to their diameter d_c such that their volume-equivalent diameter equals the diameter of the spheres in the bed of spherical particles: $d_c = \ell_c = \sqrt[3]{2/3}\, d_b$. The number of cylinders is the same as the number of spheres. We start building the cylinders bed by first building a bed of spheres – in the same way as above – of diameter $\sqrt{2}\, d_c$. Once we have this bed, the spheres are replaced by randomly oriented cylinders. The cylinders do not overlap given the diameter of the spheres they replace. This bed of cylinders is far from randomly close packed. We therefore let it settle through liquid – with a bottom layer of cylinders held fixed – until we reach a steady bed height. That bed is subsequently used for studying its interaction with an alien particle falling onto it see Fig. 1, right panel. As can be seen from the higher surface level of the granular bed of cylinders in Fig. 1, it has a lower solids volume fraction as compared to the loosely packed bed of spheres.

A base-case simulation with a bed of spherical particles has been defined. It has input parameters as listed in Table 1. The resolution of the base-case simulation is such that the diameter of the spherical bed particle spans 16 lattice spacings: $d_b/\Delta = 16$. One viscous time scale spans 25,600 time steps: $d_b^2/(\nu\Delta t) = 25,600$. For the base-case, the Reynolds number at impact is $\mathrm{Re}_i = 350$.

By matching the dimensionless numbers of a simulation system (Archimedes number, density ratios, and aspect ratios) with those of a physical system we warrant the equivalence of the two systems.

A number of variations from the base-case have been considered. (1) The effect of the size of the domain in horizontal directions has been investigated; (2) also horizontally oriented cylinders falling on the bed have been considered; (3) the density of the alien particle has been varied; (4) friction coefficients have been varied; (5) granular beds of short cylinders have been compared to beds of spheres.

5. Results

5.1. Base-case

The particle configuration at the start of the base-case simulation is shown in Fig. 1, left panel. The level of the upper surface of the particle bed is measured by taking the average z location of the centers of the ten upper most particles. This upper level is at $z_{bs} = 16.1d_b$. With $nx = ny = 16d_b$ and 4850 spheres constituting the bed, the solids volume fraction in the bed is approximately $\phi = 0.62$. At the moment the cylindrical particle is released, all particles and the liquid have zero velocity. The cylinder then falls through the liquid towards the bed under the influence of gravity. At the moment the cylinder gets for the first time in contact with a bed particle it has a velocity such that the impact Reynolds number $\mathrm{Re}_i = |u_{zi}|d_a/\nu = 350$. This moment is visualized in the left panel of Fig. 3. The subsequent panels show the cylinder sinking in the bed and slowing down, falling to one side and coming to a standstill and leaving a minor crater in the bed. In the far right panel of Fig. 3 also the liquid flow has died out. This whole process takes a dimensionless time of less than $t|u_{zi}|/d_a \approx 100$. If this is translated to the physical system described above with a bed of $d_b = 1$ mm particles, $d_a = 2$ mm and a watery liquid, one finds $|u_{zi}| \approx 9$ cm/s and $t \approx 2$ s.

In Fig. 4 the settling process is represented in time series: vertical location, vertical velocity, and orientation angle of the cylinder relative to the vertical direction as a function of time. Fig. 4 shows three realizations of the base-case. It is the same cylinder falling on the same bed of spheres and from the same height but the initial cylinder position is displaced by $\pm 4d_b$ in the x-direction. The variability between the cases is a result of the randomness of the bed. The cylinder diameter is only twice as large as the bed particle diameter so that the vertically settling cylinder initially interacts only with a few bed particles the location of

Table 1
Dimensionless input parameters of base-case.

Ar	Archimedes number $\mathrm{Ar} = (\gamma - 1)gd_a^3/\nu^2$	$1.1{\cdot}10^5$
γ	density ratio alien particle over liquid ρ_a/ρ	2.0
ρ_b/ρ	density ratio bed particle over liquid	1.1
ℓ_a/d_a	aspect ratio of (cylindrical) alien particle	4.0
d_b/d_a	bed particle diameter over alien particle diameter	0.50
μ_{bb}, μ_{ab}	friction coefficients bed-bed and alien-bed particles	0.25, 0.25
h/d_b	alien particle release height over bed particle diameter	3.62
$nx{\cdot}ny{\cdot}nz/d_b^3$	domain size relative to bed particle diameter	16·16·28

in the base-case the bed particles are spherical and the alien particle is released vertically

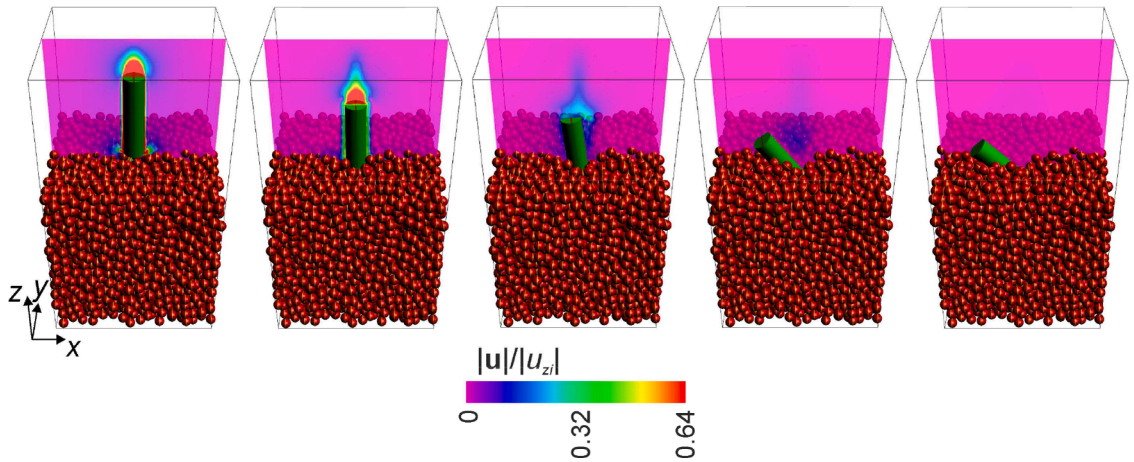

Fig. 3. Instantaneous realizations of the base-case simulation. From left to right at moments $t|u_{zi}|/d_a = 3.1$, 5.2, 10.3, 30.9, and 106. The color contours indicate liquid velocity magnitude scaled by the impact velocity $|u_{zi}|$ in the mid-plane $y = ny/2$.

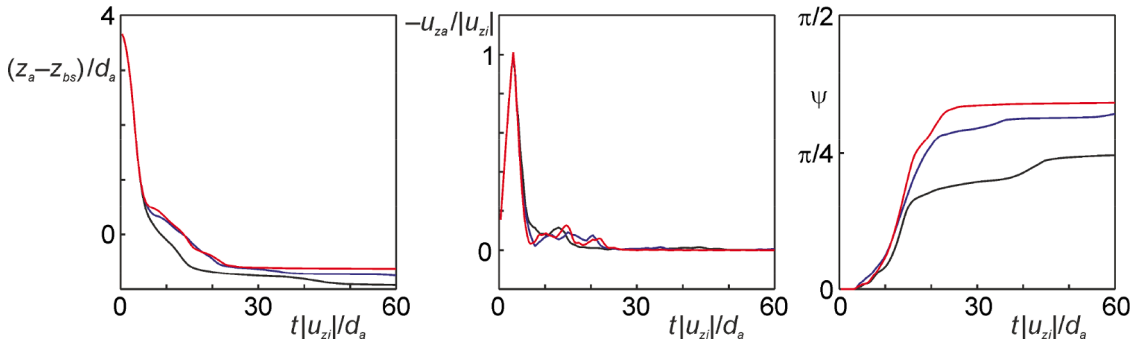

Fig. 4. From left to right: time series of the vertical location of the center of the cylinder z_a, its vertical velocity u_{za}, and its angle ψ with the vertical. The level of the undisturbed bed surface is z_{bs}. The three curves in each panel are three realizations of the settling process with the cylinder falling on the same bed of spheres. Black: situation as in Fig. 3; red and blue: cylinder initial position displaced over $\pm 4d_b$ in x-direction. Base-case conditions.

which is random in nature. Later in this paper we will see that the variability is much less if the cylinder is oriented horizontally and then interacts with many more bed particles when it lands on the surface of the granular bed.

5.2. Effect of friction coefficients

We expect that the way the alien cylinder gets stuck in the bed of spheres depends on the friction between the spheres (friction coefficient μ_{bb}) and friction between the cylinder and the bed spheres (friction coefficient μ_{ab}). Fig. 5 shows the fate of the vertically settling alien cylinder in the granular bed for four (μ_{bb}, μ_{ab}) combinations. One observes what is to be expected: lower friction coefficients lead to deeper burial of the cylinder in the bed. Also the final orientation of the cylinder relates to friction. The lesser penetration into a higher friction bed makes that the cylinder falls over sooner often leading to a larger eventual angle between the cylinder and the vertical direction. The two left panels of Fig. 5 with $(\mu_{bb} = 0.15, \mu_{ab} = 0.25)$ and $(\mu_{bb} = 0.15, \mu_{ab} = 0.15)$ show that there only is a minor effect of μ_{ab}. Fig. 6 quantifies the eventual depth of the cylinder $s = z_{bs} - z_{a\infty}$ (with $z_{a\infty}$ the eventual z-coordinate of

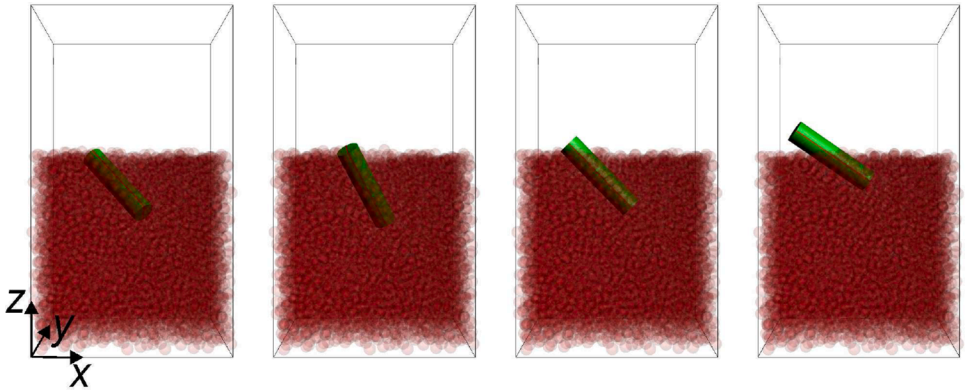

Fig. 5. Eventual position of particles as a function of friction coefficients. From left to right: $\mu_{bb} = \mu_{ab} = 0.15$; $\mu_{bb} = 0.15$, $\mu_{ab} = 0.25$; $\mu_{bb} = \mu_{ab} = 0.25$ (base case); $\mu_{bb} = 0.5$, $\mu_{ab} = 0.25$. The spheres forming the bed are made semi-transparent so as to be able to see the alien particle.

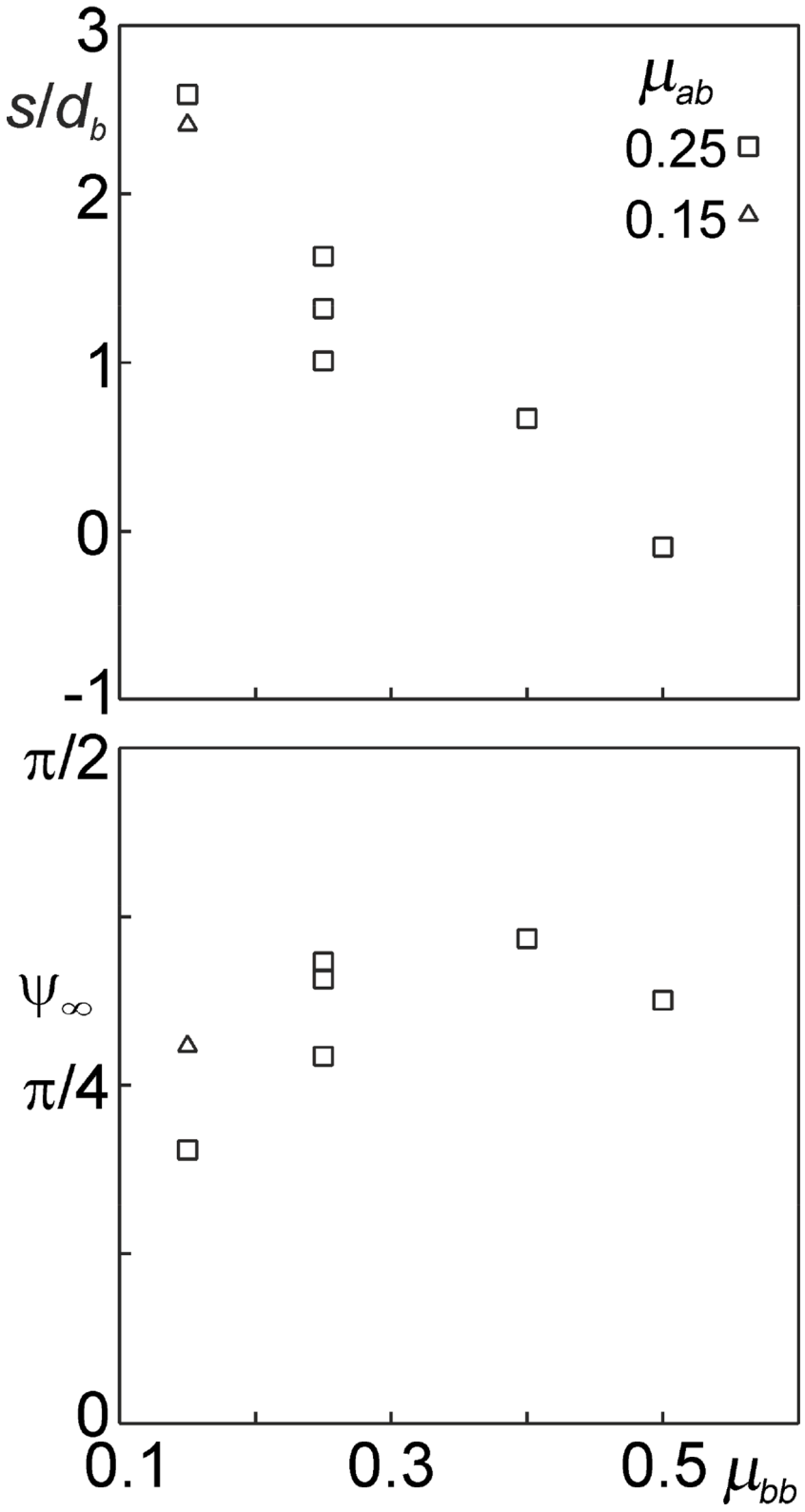

Fig. 6. Depth of the final location of the particle $s = z_{bs} - z_{a\infty}$ (top) and eventual angle with the vertical Ψ_∞ (bottom) as a function of the friction coefficient between bed particles μ_{bb}. Friction coefficient between alien particle and bed particle μ_{ab} as indicated.

the center of the alien particle) and its eventual angle with the vertical Ψ_∞ as a function of μ_{bb} confirming the trend of deeper burial with lower friction and a – admittedly less clear – increase of angle with higher friction. Fig. 6 includes the three realizations reported in Fig. 4 with $(\mu_{bb} = 0.25, \mu_{ab} = 0.25)$and gives a sense of the variability of the eventual depth and angle as a result of the location of impact of the vertically oriented cylinder on the random bed.

5.3. Horizontal cylinder

We now change the initial orientation of the cylinder from vertical to horizontal. The bed on which the cylinder settles is the same bed of spherical particles as in the simulations discussed above that involved a vertical cylinder. In this set of simulations the focus is on the effect of the density of the alien particle. Density ratios $\gamma = \rho_a/\rho$ are in the range 2 to 6 while keeping$\rho_b/\rho = 1.1$. Impressions of the eventual position of the cylinder are in Fig. 7. In the three cases shown in that figure the cylinder does not get fully buried, i.e. it can still be seen looking from the top. In case $\gamma = 6$ (not shown in Fig. 7) the cylinder gets buried. Given that the side views show spheres at higher locations than the cylinder implies that a shallow crater has formed on the bed.

Depth as a function of density ratio γ shows a steeply increasing depth with increasing density ratio, see Fig. 8. Additionally, Fig. 8 contains information on reproducibility and the effect of the friction coefficient. Three simulations were conducted for $\gamma = 4$ and $\mu_{aa} = \mu_{ab} = \mu = 0.25$ with the cylinder falling on different locations of the granular bed. The variability of the eventual depth of these realizations is much less than for a vertically settling cylinder (compare with Fig. 6) which is easy to understand. Initially the horizontal cylinder is interacting with many more bed particles as compared to the vertical cylinder so that random bed effects are evened out much more and the settling process is less sensitive to the location on the bed.

As before for vertical cylinders, friction is a much determining concept. In the set of simulations presented in Fig. 8 we have been using a single friction coefficient $\mu = \mu_{aa} = \mu_{ab}$. For $\gamma = 4$, the depth for $\mu = 0.15$ is approximately five times larger than the depth for $\mu = 0.5$.

5.4. Lateral domain size

As stated above, periodic boundary conditions apply in the lateral (x and y) directions with a base-case domain size of $nx = ny = 16d_b$. The alien cylinder has diameter $d_a = 2d_b$ and length $\ell_a = 8d_b$ which are appreciable fractions of the lateral size of the domain. We thus need to investigate if the lateral domain size has an influence on the way the alien particle settles on (and through) the bed and on its eventual depth. Given that in the simulations shown so far the cylinder comes to rest at least $10d_b$ above the bottom of the domain we do not anticipate a significant effect of the vertical domain size.

In addition to the already reported cases, simulations have been performed for a vertical cylinder of base-case size with $\gamma = 2$ settling in beds with $nx = ny = 8d_b$ and $nx = ny = 24d_b$, as well as for a horizontal cylinder with $\gamma = 4$ in beds with $nx = ny = 24d_b$. Results in terms of eventual depth are given in Fig. 9. The figure also contains the results reported in Figs. 6 and 8 that show the variability of the depth if the same cylinder lands on different locations on the bed. Fig. 9 shows a consistent increase of depth with increasing domain size – an effect that goes beyond (random) bed variability. The increase in depth can be explained by the bed rising as a result of bed particles being displaced by the cylinder and the crater it forms where it should be noted that the depth s is defined based on the undisturbed bed height. In addition, particularly for horizontal cylinders, we expect an increased level of hindrance over the periodic boundaries in smaller domains.

5.5. Cylindrical particles bed

To investigate the effect of the shape of bed particles, a bed of short cylinders was created, see Fig. 1 (right panel). Each particle in this bed

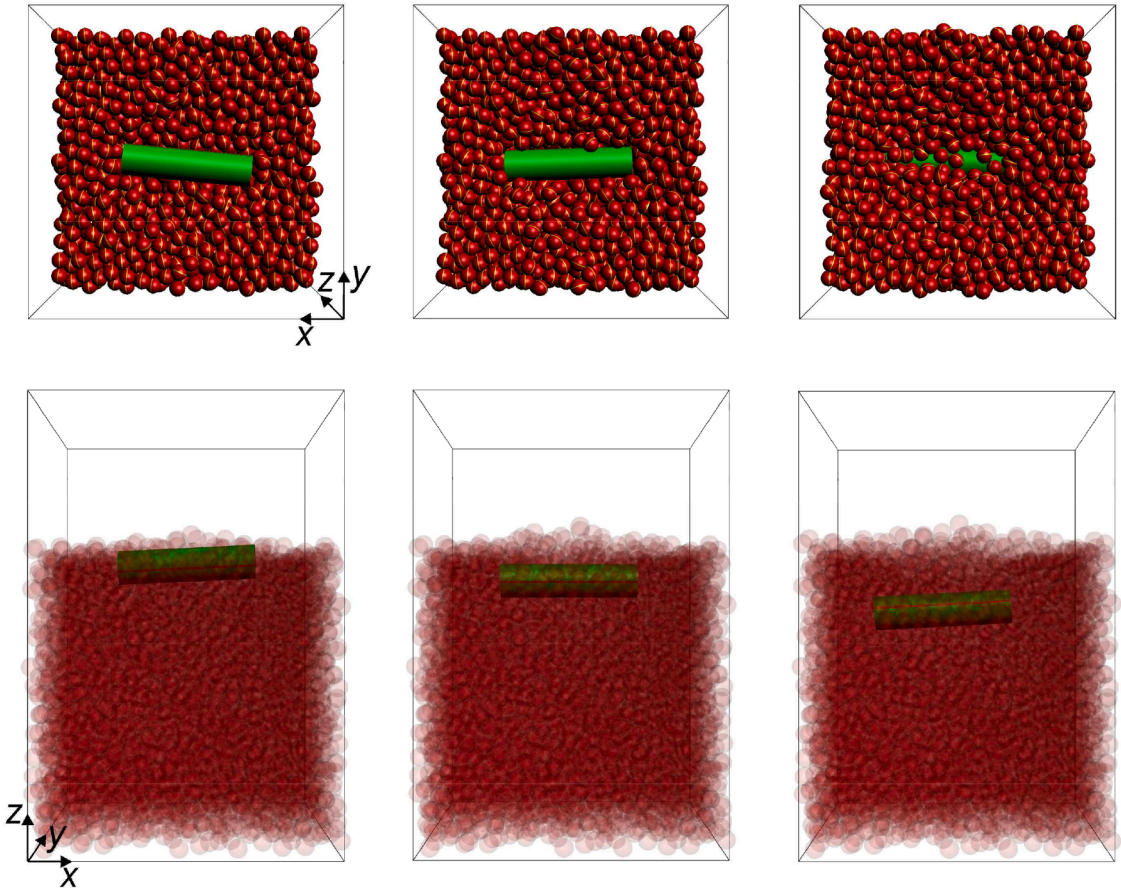

Fig. 7. Eventual particle configuration for a horizontally settling cylinder with density ratio $\gamma = 2$, 3, 4 (from left to right). Top row: top view; bottom row: side view with semi-transparent spheres. The Reynolds numbers at impact are $\mathrm{Re}_i = |u_{zi}|d_a/\nu$=310, 420, and 480 respectively.

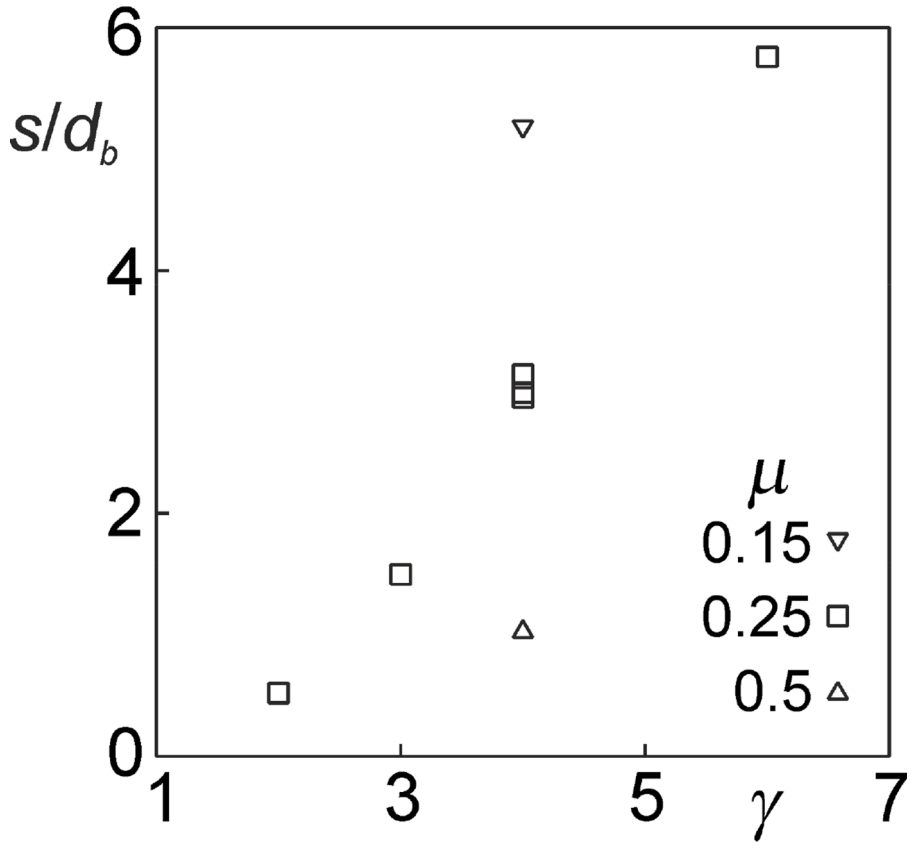

Fig. 8. Eventual depth s of the cylinder after settling horizontally as a function of the density ratio γ. In these simulations $\mu_{bb} = \mu_{ab} = \mu$ with μ as indicated.

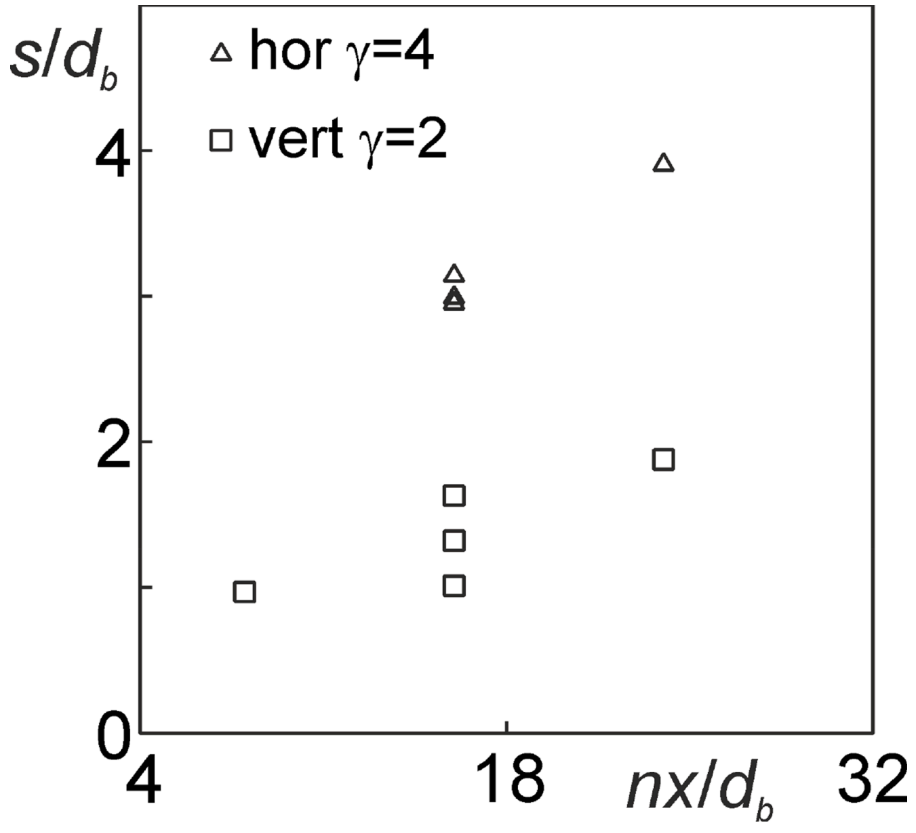

Fig. 9. Domain size effects on the depth s of the alien cylinder at the end of the settling process. Data for a horizontally settling alien cylinder with $\gamma = 4$, and a vertically settling cylinder with $\gamma = 2$. Note that $nx = ny$ in all simulations.

has the same volume as a spherical bed particle, and the two beds contain the same number of particles. Given that the bed of cylinders is higher means that – by settling through liquid – we have achieved a lower solids volume fraction: $\phi = 0.55$ (versus 0.62 for the bed of spheres).

Impressions of the settling of an alien horizontally oriented cylinder on this bed are shown in Fig. 10. Fig. 11 shows the eventual location in the bed of cylinders of an alien cylinder with $\gamma = 4$ entering the bed horizontally and a vertically oriented cylinder with $\gamma = 2$ respectively. The depths are $s = 8.19d_{be}$ for the horizontal cylinder and $s = 2.89d_{be}$ for the vertical cylinder respectively where d_{be} is the equivalent diameter of the bed particles which is equal to the diameter of the spherical bed particles ($d_{be} = d_b$). We compare this with the same cylinders settling horizontally and vertically in the bed of spheres. For these we had three realizations each with an average depth of $\bar{s} = 3.03d_b$ (horizontal, $\gamma = 4$) and $\bar{s} = 1.32d_b$ (vertical, $\gamma = 2$) respectively. Hence, the alien cylinders penetrate significantly deeper in the bed of short cylinders. This is despite the fact that the impact Reynolds numbers are slightly lower for the settling on the cylinders bed given that that bed is higher than the bed of spheres and the alien cylinders is released at the same location in the domain so that it accelerates less before touching the bed surface. We note that the cylinders bed is much looser (has a much lower solids volume fraction) than the spheres bed which might be a factor very relevant to the penetration depth.

To further investigate the latter hypothesis, a denser bed of short cylinders was created. This was done by numerically shaking the original bed of $\phi = 0.55$ in the horizontal direction for an extensive amount of time. Horizontal numerical shaking is achieved by imposing a periodic (sinusoidal) acceleration in a horizontal direction (x-direction in this case) to the particles. With an amplitude of the horizontal acceleration equal to the magnitude of gravitational acceleration and a period time of $\sim 20\sqrt{d_{be}/g}$ the solids volume fraction of the bed could be increased from $\phi = 0.55$ to 0.59. A horizontal cylinder with $\gamma = 4$falling in this bed reaches a depth of $s = 2.5d_{be}$ which is slightly smaller than the depth the same cylinder reached in the bed of spheres with $\phi = 0.62$ (same friction coefficients in the two cases). Settling in the loose and

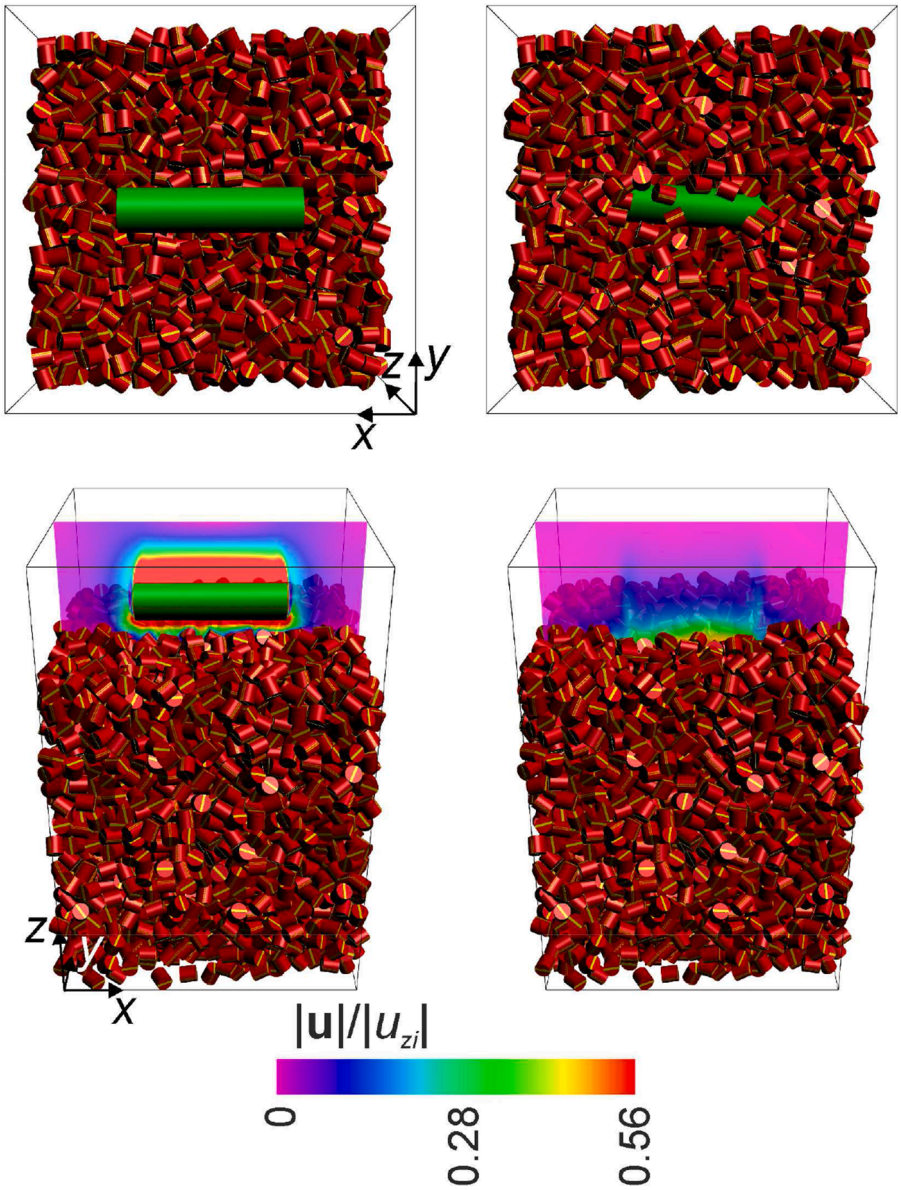

Fig. 10. Two instantaneous realizations of a horizontal alien cylinder with $\gamma = 4$ settling in a granular bed of short cylinders. The Reynolds number at impact is $\mathrm{Re}_i = |u_{zi}|d_a/\nu = 400$. Top row: top view; bottom row: side view. Left: $t|u_{zi}|/d_a = 2.7$; right: $t|u_{zi}|/d_a = 7.8$. The color contours in the lower panels indicate liquid velocity magnitude scaled by the impact velocity $|u_{zi}|$ in the mid-plane $y = ny/2$.

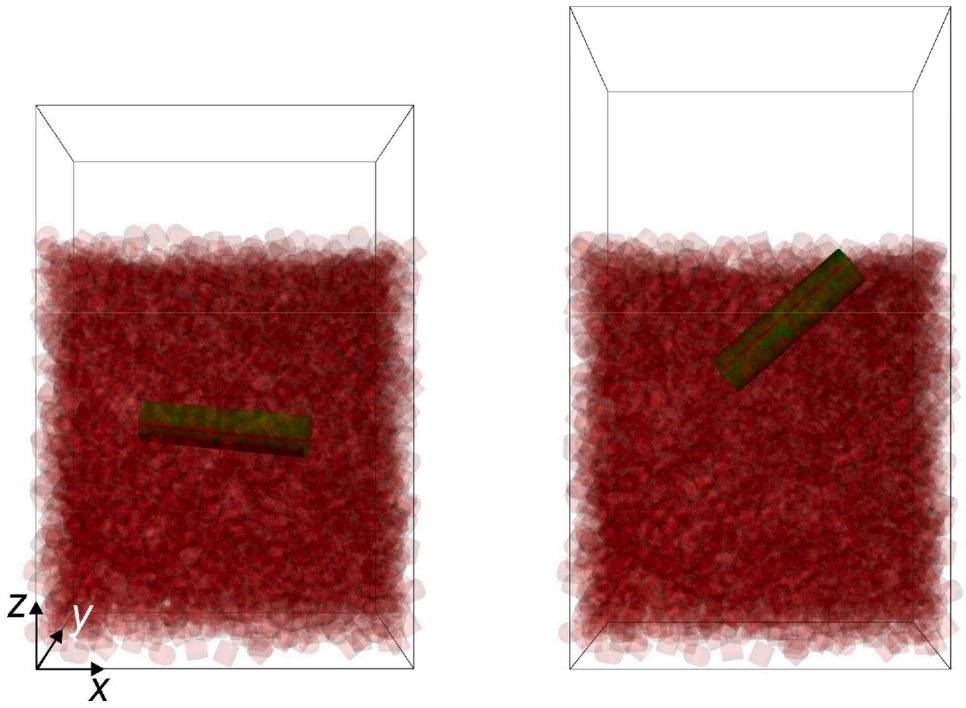

Fig. 11. Eventual position of the alien cylindrical particle in a bed of short cylinders. Left: an initially horizontally oriented alien cylinder with $\gamma = 4$; right : an initially vertically oriented alien cylinder with $\gamma = 2$.

dense cylinder beds are further compared in terms of time series of the vertical position of the alien particle in Fig. 12.

6. Conclusions

This paper reports on particle-resolved simulations of an "alien" particle intruding in a liquid-saturated granular bed. The alien particle is a heavy cylinder with length over diameter aspect ratio 4 falling towards the bed either vertically or horizontally. As the main outcome metric, the depth of penetration in the granular bed has been considered. Dependencies of the depth of penetration on alien particle density, friction coefficients and domain size have been investigated. In this respect, the dependency on friction coefficients is the most interesting one. This is not only because it is a very strong dependency. Friction coefficients are parameterizations of physical processes occurring at the length scale of surface roughness which is a length scale not resolved by the

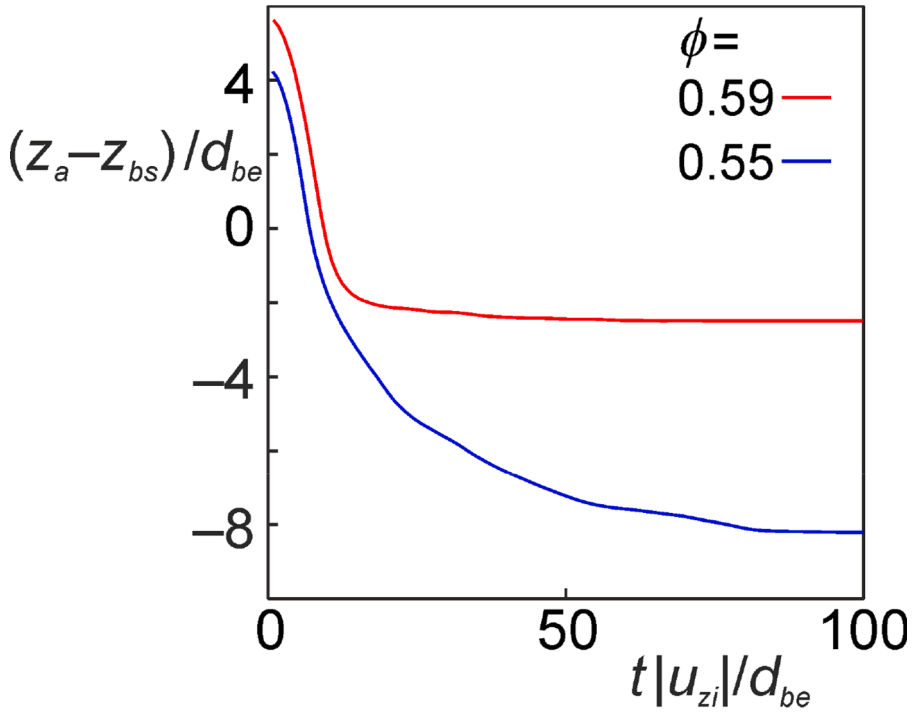

Fig. 12. Time series of the vertical location (z_a) of the center of a horizontal alien cylinder with $\gamma = 4$ falling on a bed of short cylinders. The undisturbed bed surface is at vertical location z_{bs}. Comparison between two beds with undisturbed solids volume fractions ϕ as indicated.

simulations. To apply the simulation methodology to real systems one thus needs experimental input: either direct measurement of friction coefficients, or experiments for which the outcome critically depends on friction, such as the cases that have been studied in this paper.

As expected, the simulations showed that a denser cylinder sinks deeper in the granular bed. The dependency of penetration depth on domain size relates to computational cost. We have been applying periodic boundary conditions in the horizontal directions which mean that we are in principle simulating an infinite two-dimensional array of identical systems. The increase of penetration depth with domain size teaches that these periodic copies hinder one another so that we need larger domains – and thus many more bed particles – to be able to significantly reduce such hindrance over the periodic boundaries.

The results achieved with granular beds of spherical particles have been compared to two beds comprised of short cylinders. A relatively loose bed of $\phi = 0.55$ was created by letting the cylinders settling though liquid; after shaking that bed a second, denser bed with $\phi = 0.59$ is formed. In the looser bed an alien cylinder penetrated much deeper than in a bed of spheres with $\phi = 0.62$. Interestingly, the alien cylinder settles slightly less deep in a bed of short cylinders with $\phi = 0.59$ than it does in a bed of spheres of $\phi = 0.62$.

There are various avenues for future research. First and foremost we would like to advocate experimental work for validation and guidance of the simulations. The systems we have simulated are simple. They do require care in – for instance – selecting spherical particles with a very narrow size distribution as well as accurately measuring penetration depth. In terms of selection of particles, one option would be to use polyoxymethylene (POM) spheres (Penick et al., 2005).

Another avenue for future work is to include flow over the bed to study how entrainment of an alien particle by fluid flow affects the scenario of its interaction with the granular bed.

CRediT authorship contribution statement

J.J. Derksen: Conceptualization, Methodology, Visualization, Investigation, Writing – original draft, Writing – review & editing.

Declaration of Competing Interest

The author declares that they have no known competing financial interests or personal relationships that could have appeared to influence the work reported in this paper.

Acknowledgement

Inspiration for the research described in this paper came from discussions with my colleagues Tom O'Donoghue and Dominic van der A of the Fluid Mechanics Research Group of the School of Engineering of the University of Aberdeen.

References

Derksen, J.J., 2019. Liquid fluidization with cylindrical particles: Highly resolved simulations. AIChE J 65 pe16594–1–11.
Derksen, J.J., "Liquid co-fluidization of cylinders and spheres," Canadian J. Chem. Eng. in press (2022).
Derksen, J.J., Sundaresan, S., 2007. Direct numerical simulations of dense suspensions: wave instabilities in liquid-fluidized beds. J. Fluid Mech. 587, 303–336.
Hill, R.J., Koch, D.L., Ladd, A.J.C., 2001. Moderate-Reynolds-number flows in ordered and random arrays of spheres. J. Fluid Mech. 448, 243–278.
Kidanemariam, A.G., Uhlmann, M., 2014. Interface-resolved direct numerical simulation of the erosion of a sediment bed sheared by laminar channel flow. Int. J. Multiph. Flow 67, 174–188.
Kidanemariam, A.G., Uhlmann, M., 2017. Formation of sediment patterns in channel flow: minimal unstable systems and their temporal evolution. J. Fluid Mech. 818, 716–743.
Kruger, T, Kusumaatmaja, H, Kuzmin, A, Shardt, O, Silva, S, Viggen, EM., 2017. The Lattice Boltzmann Method: Principle and Practice. Springer.
Kuipers, J.B., 1999. Quaternions and Rotation Sequences. Princeton University Press, Princeton.
Nguyen, N.-Q., Ladd, A.J.C., 2002. Lubrication corrections for lattice-Boltzmann simulations of particle suspensions. Phys. Rev. E 66, 046708.
Penick, K.J., Solchaga, L.A., Berilla, J.A., Welter, J.F., 2005. Performance of polyoxymethylene plastic (POM) as a component of a tissue engineering bioreactor. J. Biomed. Mater. Res. A. 75, 168–174.
Rubinstein, G.J., Derksen, J.J., Sundaresan, S., 2016. Lattice Boltzmann simulations of low-Reynolds-number flow past fluidized spheres: effect of Stokes number on drag force. J. Fluid Mech. 788, 576–601 vol. 788(2016).
Shardt, O., Derksen, J.J., 2012. Direct simulations of dense suspensions of non-spherical particles. Int. J. Multiphase Flow 47, 25–36.
Somers, J.A., 1993. Direct simulation of fluid flow with cellular automata and the lattice-Boltzmann equation. Appl. Sci. Res. 51, 127–133.
Succi, S., 2001. The Lattice Boltzmann Equation for Fluid Dynamics and Beyond. Clarendon Press, Oxford.
Ten Cate, A., Nieuwstad, C.H., Derksen, J.J., Van den Akker, H.E.A., 2002. PIV experiments and lattice-Boltzmann simulations on a single sphere settling under gravity. Phys. Fluids 14, 4012–4025.
Torquato, S., Truskett, T.M., Debenedetti, P.G., 2000. Is random close packing of spheres well defined? Phys. Rev. Lett. 84, 2064–2067.
Uhlmann, M., 2005. An immersed boundary method with direct forcing for the simulation of particulate flows. J. Comput. Phys. 209, 448–476.
Van der Hoef, M.A., Beetstra, R., Kuipers, J.A.M, 2005. Lattice-Boltzmann simulations of low-Reynolds-number flow past mono- and bidisperse arrays of spheres: results for the permeability and drag force. J. Fluid Mech. 528, 233–254.
Vowinckel, B., Nikora, V., Kempe, T., Frohlich, J., 2007. Spatially-averaged momentum fluxes and stresses in flows over mobile granular beds: a DNS-based study. J. Hydraul. Res. 55, 208–223.
Wachs, A., 2009. A DEM-DLM/FD method for direct numerical simulation of particulate flows: sedimentation of polygonal isometric particles in a Newtonian fluid with collisions. Comput. Fluids 38, 1608–1628.
Wachs, A., 2019. Particle-scale computational approaches to model dry and saturated granular flows of non-Brownian, non-cohesive, and non-spherical rigid bodies. Acta Mech 230, 1919–1980.
Wylie, J.J., Koch, D.L., Ladd, A.J.C., 2003. Rheology of suspensions with high particle inertia and moderate fluid inertia. J. Fluid Mech. 480, 95–118.
Yamamoto, Y., Potthoff, M., Tanaka, T., Kajishima, T., Tsuji, Y., 2001. Large-eddy simulation of turbulent gas–particle flow in a vertical channel: effect of considering inter-particle collisions. J. Fluid Mech. 442, 303–334.
Yan, Z., Wilkinson, S.K., Stitt, E.H., Marigo, M., 2015. Discrete element modelling (DEM) input parameters: understanding their impact on model predictions using statistical analysis. Comp. Particle Mech. 2, 283–299.